

# QUENCH AND FIELD EMISSION DIAGNOSTICS FOR THE ESS MEDIUM-BETA PROTOTYPES VERTICAL TESTS AT LASA

M. Bertucci<sup>†</sup>, A. Bellandi, A. Bignami, A. Bosotti, J.F. Chen, P. Michelato, L. Monaco,  
R. Paparella, D. Sertore, INFN–LASA, Segrate (MI), Italy  
C. Pagani, University of Milano & INFN-LASA, Milano, Italy  
S. Pirani, ESS, Lund, Sweden and on leave at INFN-LASA, Segrate (MI), Italy

## Abstract

In order to investigate the possible causes of premature thermal breakdown and performance degradation, several diagnostic techniques have been employed during the vertical tests of the Fine and Large Grain ESS Medium Beta prototypes cavities. The whole equipment, which includes second sound, fast thermometry, photodiode x ray detectors and external NaI scintillator and proportional counter, is here described and the results so far obtained during the vertical tests presented.

## INTRODUCTION

In the framework of the ESS activity in progress at INFN-LASA, two prototype 704.42 MHz medium beta ( $\beta=0.67$ ) have been designed [1] and produced [2]. The two cavities have the same geometry but different materials: the first in Fine grain (FG) and the second in large grain (LG) niobium. The aim of this is to investigate and compare the material performances and possibly highlight the technical benefits of LG niobium.

Two main mechanisms may cause the premature collapse, a.k.a. quench, of cavity performance. The first is thermal breakdown (TB) due to a local anomalous heat generation driving a part of cavity niobium surface above the critical temperature and thus generating a temperature instability. The quench origin is usually a non-superconducting material contamination but can be also due to magnetic field enhancement, at microstructures on the RF surfaces or on the grain boundary steps in the LG case. [3,4]

The second mechanism is field emission (FE), where the creation of a “dark current” parasitically adsorbs RF power, leading to the declining of  $Q_0$  and causing the production of heat and x-ray radiation due to electron impact on cavity walls. Moreover, if the emission from a single site is intense, the heat generated by impacting electrons on high magnetic field regions can generate a thermal breakdown event [5]. FE is generated by impurities on cavity walls (like dust or metallic contaminations) or by local asperities on the niobium surface itself.

In view of the vertical tests foreseen at the LASA facility, several diagnostic techniques have been installed so to investigate and detect the physical processes accountable for any possible performance limitation. According to the previous classification, we divide them in the two categories of TB and FE detectors.

## QUENCH EVENTS DETECTION

TB usually occurs in region of high magnetic fields, namely in a zone extending from equator up to 4.8 cm toward the iris, according to Fig. 1 which shows the surface electric and magnetic field cavity profile reconstructed by Superfish.

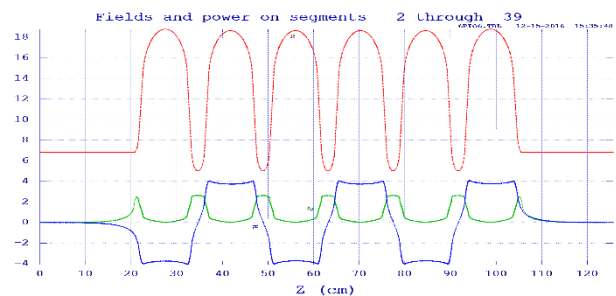


Figure 1: Superfish reconstruction of surface electric (green) and magnetic (blue) fields along cavity axis.

The techniques of quench detection give their best if combined with cavity visual inspection, usually performed after cavity heat treatment, and pass-band mode analysis which give a preliminary indication of quenching cells [6].

## Second Sound

20 Oscillating Superleak Transducers (OST) sensors [7] are installed on a frame surrounding the cavity external surface. The geometrical arrangement is chosen so that every surface point is covered by at least 4 lines of sight point-to-sensor paths. The signals from OST emerge from the cryostat by SMA-vacuum feedthroughs and are processed by a multichannel amplifier which supplies a 27 dB gain up to 100 kHz and also provides a 90V polarization to OST membranes. The amplified signals are then collected by a National Instruments Compact Rio acquisition unit. The trigger is obtained by digitalization of transmitted power signal so that acquisition is synchronous with cavity quench. The collected data are analysed with Labview VIs exploiting several algorithms of trilateration [6]. According to our experience, a 1-2 cm resolution for quench localization is achievable with second sound.

## Fast Thermometry

The process of TB on cavity inner surface produces in its turn a great dissipation of heat on the Nb-He interface, eventually producing an external temperature increase, once again synchronous with the drop of cavity transmit-

<sup>†</sup> email address      michele.bertucci@mi.infn.it

ted power. Thermometry sensors (Cernox® and CCS®) with fast readout electronics are attached to the cavity surface, with a four-wire configuration to read the resistance of the sensor. A FET low current generator able to provide 10 or 100  $\mu\text{A}$  of stable current feeds each sensor. A low noise amplifier and a National Instruments PCI-6281 fast acquisition board (18 Analog Input, 625 kS/s) acquire the sensor signals.

## FIELD EMISSION DETECTION

Although FE is produced on irises, the multiple electron trajectories will generate bremsstrahlung x-rays potentially everywhere on cavity surface. Simulations are now underway with ASTRA, CST and HFSS to investigate the possible trajectories and impact energies of field emitted electrons and will be published in a future work. In Fig. 2 the possible electron trajectories generated by a field emitter on iris 3 are shown for the accelerating field of 17 MV/m. The impact energy of electron hitting the beam-pipe is 8 MeV. Attenuation of X-ray radiation emerging from the cryostat can be evaluated as  $I/I_0 = \exp(-\mu D)$ . Assuming  $D=55$  mm as total thickness (20 mm of beam pipe flange + 35 mm of cryostat cover), and  $\mu = 0.235 \text{ cm}^{-1}$  for the linear absorption coefficient of iron at 8 MeV [8], we obtain  $I/I_0 = 0.27$  so that the field-emitted X-ray radiation is barely attenuated to one fourth of its initial intensity despite the crossing of several cm of steel. The radiation emerging from the cryostat can therefore yield a substantial indication on highly energetic FE events occurring in the cavity.

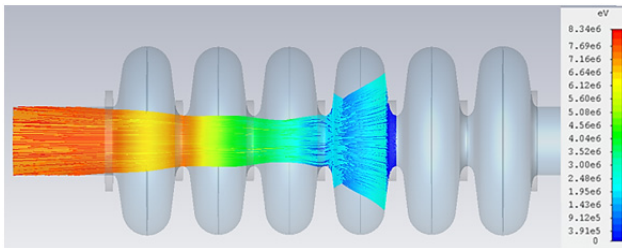


Figure 2: electron trajectories of cavity FE at 17 MV/m. The colour gives the energy scale.

## External Radiation Dose and Energy

A proportional counter (Thermo Electron FH 40-G) is installed outside of the cryostat along the cavity axis. The instrument measures the equivalent dose rate in Sv/h, with a measuring range from 100 nSv/h to 1 Sv/h. During the test, the dose rate is acquired continuously every second. This can offer a first estimate of FE yield albeit the emitted current cannot be directly extrapolated without any further information on produced X-ray energy spectrum.

Aiming to measure the latter, a NaI(Tl) scintillation detector (Ortec 905-4) is installed beside the proportional counter. The detector has a 2''x2'' cylindrical active volume and can sustain up to a 100000 count/sec rate without suffering significant pulse pile-up. It is equipped with an Ortec digiBASE unit, integrating the photomultiplier HV supply, the preamplifier and a 1024 channel

MCA. The energy spectrum is acquired with MAESTRO® software. Energy calibration is performed with  $^{137}\text{Cs}$  (0.662 MeV) and  $^{60}\text{Co}$  (1.173 MeV and 1.332 MeV) gamma lines.

## Photodiode Detectors

4 photodiode detectors are installed inside the cryostat for monitoring the radiation produced by FE. Differently from the external radiation measurements, a more direct evaluation of real radiation yield can be in this way potentially obtained, avoiding indirect contributions due to Compton scattering on cryostat walls and granting a more accurate localization of electron impact points. The drawback is the more compelling context (liquid helium bath at 2 K) limiting the performances of amplifiers electronics. For this reason, photodiode amplification is generally carried out outside the cryostat but this introduces pickup noise due to longer cables. A different strategy is here exploited, developing an *ad hoc* amplifier board suitable in the cryogenic context. Above all, a CMOS-based OPamp (ICL7621) is used instead of traditional BJT components. The former can operate at low temperatures without suffering of the rapid decline in gain of the latter [9]. The PiN diode employed is Hamamatsu S1223-01, amongst all considered the best performing in terms of cost and signal to active area ratio [10]. The amplifier circuit, outlined in Fig. 3, is a transimpedance amplifier whose first-stage output voltage  $V_1 = -R_f i_d$  is then amplified by second stage closed loop gain  $V_2 = -(R_{f2}/R_1)V_1$ . A low pass filter completes the amplification chain.

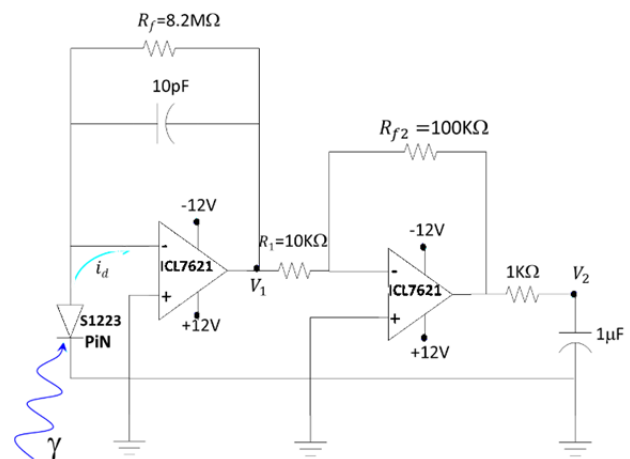


Figure 3: Photodiode amplifier circuit.

## RESULTS ON CAVITY TESTS

The experimental data obtained from diagnostics are here presented. For more details on the cavity test refer to [11]. All here mentioned measurements are done at the maximum  $E_{\text{acc}}$ , unless otherwise specified. In sake of conciseness, the details of measurements are explicitly shown only if considered particularly relevant.

### Fine Grain Cavity

ESS FG cavity reached a maximum  $E_{acc}=22.2$  MV/m before quenching. A confined quench zone on cavity surface has been detected unequivocally by second sound. In the same time FE has been detected: the proportional counter measured a maximum dose of 200  $\mu\text{Sv/h}$ , while the scintillator measured an endpoint of 2.5 MeV at 21.5 MV/m. At quench field, the detector suffered of pulse pileup due to high radiation rate. The readout of photodiodes are reported in Fig. 4 together with external radiation. In the box, external radiation and  $E_{acc}$  are fitted by means of Fowler-Nordheim relation:

$$J(E_p) \propto (\beta E_p)^{2.5} \exp(-6.1 \cdot 10^4 / \beta E_p)$$

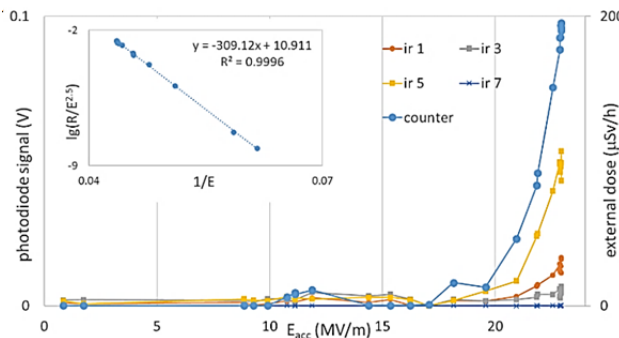


Figure 4: photodiode signals vs  $E_{acc}$ , labelled with corresponding cavity irises, and external radiation level.

The cavity has been then tested after tank integration, with further BCP and 24h HPR resetting the surface state. The cavity reached the same  $E_{acc}$  without suffering FE.

### Large Grain Cavity

LG cavity reached a maximum  $E_{acc}=10$  MV/m before quenching. Even this time, a localized TB is detected by second sound together with high degree of radiation measured by external detectors and photodiodes. Then the cavity has been tested in all the 6 passband modes and the second sound analysis, cross checked with modal analysis, confirmed the occurrence of three different quench points. Figure 5 shows the reconstructed position for every

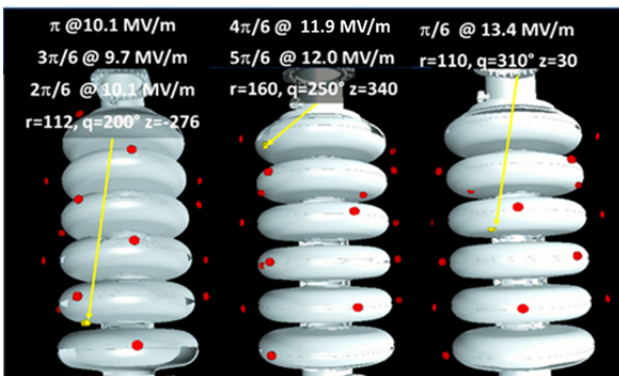


Figure 5: second sound reconstruction of the 6 passband modes quench, gathered in “same quench” families.

pass-band mode, together with maximum  $E_{acc}$  in quench cell.

By means of optical inspection, some significant grain boundary structures are identified near the quench points, albeit not particularly prominent. No significant temperature changes have been measured by Cernox.

In the first test, the external dose reached 2 mSv/h at quench. After 2 conditioning cycles, dose level reduced to 0.4  $\mu\text{Sv/h}$  but cavity still quenched at the same  $E_{acc}$ .

Figure 6 shows the scintillation spectra before and after the processing. The initial value of 5 MeV is fully compatible with the results of already mentioned CST and ASTRA simulations. At the nominal  $E_{acc}$  of 10 MV/m a maximum impact energy of 4.9 MeV is indeed obtained for electrons hitting the beam pipe flange. Endpoint energy reduces with conditioning, eventually stabilizing at 2.8 MeV. This suggests the presence of more field emitting sites on cavity surface: RF processing successfully eliminates the sites producing high energy electrons so drastically reducing the external dose level.

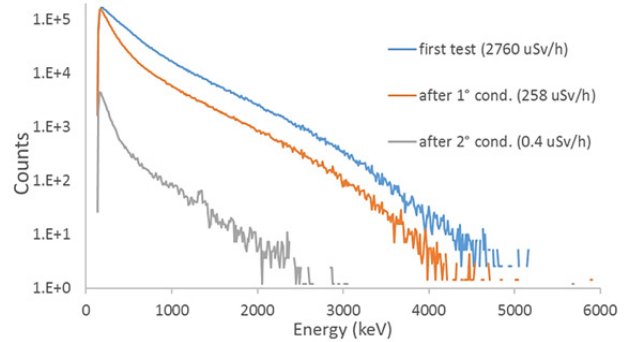


Figure 6: scintillation spectra at quench field before and after conditioning. Acquisition time is 60 sec. in all cases.

Different scenarios could explain the low cavity performances: amongst them, a possible FE induced quench. Aiming to exclude (or confirm) this hypothesis, the cavity has been tested again after a 24h HPR and 20  $\mu\text{m}$  BCP: FE disappeared but the quench occurred at the same field. Second sound detected exactly the same quenching points of the first tests. This leads us to conclude that cavity performance limitation is due to TB.

## CONCLUSIONS

The diagnostics methods here outlined allowed collecting a big amount of information during ESS cavity prototypes vertical tests, highlighting the cavity limitation mechanisms. Especially for LG cavity, we obtained precious indications about quench locations. Due to presence of grain boundaries and absence of evident particle contaminations in the quench sites, a magnetic field enhancement induced TB can be hypothesized, even if a “smoking gun” evidence of this is still lacking.

Aiming to find it, a proper strategy will be developed for the future cavity tests by choosing suitable recovering treatments, and further in-depth analysis on the data so far collected. More details on diagnostics will be given in a future work dedicated to R&D activities on LG cavity.

## REFERENCES

- [1] ESS, <https://europeanspallationsource.se>
- [2] P. Michelato *et al.*, in *Proc. IPAC '16*, pp. 2138-2140.
- [3] J. Knobloch *et al.*, *Proc. SRF '99*, pp.77-91.
- [4] T. Kubo, *Proc. SRF '13*, pp. 433-437.
- [5] H. Padamsee, *RF conductivity. Science, Technology and Applications*, Wiley and Sons, New York, 2009.
- [6] M. Bertucci *Proc. SRF '13*, pp. 704-707.
- [7] R.A. Sherlock, D. O. Edwards, "Oscillating Superleak Second Sound Transducers", *Rev. Sci. Instrum.*, vol. 41, p.1603, 1970.
- [8] NIST website, <https://www.nist.gov>
- [9] K. Hayashi *et al.*, "A current to voltage converter for cryogenics using a CMOS operational amplifier", *Journ. Ph. Conf. Series*, vol.150, p.012016, 2009.
- [10] A. D. Palczewsky and R. L. Geng , in *Proc. IPAC '16*, pp. 2438-2440.
- [11] A. Bosotti *et al.*, "Vertical Tests of ESS Medium Beta Prototype Cavities at LASA" presented at IPAC'17, Copenhagen, Denmark, May 2017, MOPVA063.